

**Supporting Information for**  
**Tunable photothermal actuators based on a pre-programmed aligned**  
**nanostructure**

*Jue Deng, Jianfeng Li, Peining Chen, Xin Fang, Xuemei Sun, Yishu Jiang, Wei Weng,  
Bingjie Wang and Huisheng Peng\**

*State Key Laboratory of Molecular Engineering of Polymers, Department of  
Macromolecular Science and Laboratory of Advanced Materials, Fudan University,  
Shanghai 200438, China; E-mail: penghs@fudan.edu.cn.*

## Supplementary Notes

### 1. Experimental section

**1.1 Impact of the void among aligned CNTs on the bending direction.** Aligned CNTs were firstly deposited on the *Teflon* film along the same direction, followed by stretching the substrate to enlarge the voids among the aligned CNTs. The actuator strips were fabricated by transporting aligned CNTs (Figure S5) onto the paraffin wax/polyimide strip. Figure S5 showed that different voids among the aligned CNTs did not affect the bending direction for both phototropic and apheliotropic bending. However, the larger voids attenuated the magnitude of deformation because less photothermal energy was absorbed by the CNTs and the tensile and contractile stresses were also lowered.

**1.2 Calculation of strain energy density.** The bending actuation can be simplified to the model of bending beam. Therefore, the strain energy density ( $V_\epsilon$ ) can be calculated by the  $V_\epsilon = M\theta / 2V$  during the elastic bending process. Here,  $M$ ,  $\theta$  and  $V$  are bending moment, bending angle and the volume, respectively. The bending moment was  $6 \times 10^{-4}$  N m, so the strain energy densities were calculated to be  $2.4 \times 10^7$  J m<sup>-3</sup> and  $1.7 \times 10^7$  J m<sup>-3</sup> for apheliotropic and phototropic bending, respectively.

**1.3 Fabrication of the fiber-shaped perovskite solar cell.** The aligned TiO<sub>2</sub> nanotube arrays grown on the surface of Ti wire were realized by an electrochemical anodization in electrolyte composed of water and glycerol (v/v, 1/1) and 0.27 M NH<sub>4</sub>F at a voltage of 20 V for 20 min. The anodization was performed in a two-electrode electrochemical cell with Ti wire (diameter of 250 μm and purity of 99.7%) and Pt sheet as anode and cathode, respectively. The resulting wires were washed with deionized water to remove the electrolyte, followed by temperature programming to 500 °C in 30 min and kept in air for 1 h. The resulting modified Ti wires were dipped into the perovskite precursor solution for 30 s and then annealed for 5 min. After repeating the dip-coating process for at least three times, the modified wires were annealed at 100 °C for 2 h. The hole transport material solution containing 0.170 M 2,2',7,7'-tetrakis (N,N-di-p-methoxyphenylamine)-9,9'-spirobifluorene (spiro-MeOTAD, Chemsy International Co., Ltd), 0.064 M bis(trifluoromethane) sulfonamide lithium salt (LiTFSI, 99.95%, Aladdin) and 0.198 M 4-tertbutylpyridine (TBP, 96%, Aladdin) in a solvent mixture of chlorobenzene (99.8%, Aldrich) and acetonitrile (99.8%, Aldrich) (v/v, 10/1) was dip-coated on the perovskite layer for 30 s in air. Finally, an aligned CNT sheet was wrapped around the wire to produce the fiber-shaped perovskite solar cell.

**1.4 Sample preparation for fluorescence microscope and laser scanning confocal microscopy measurements.** Rhodamine solution (1 mg/mL) was prepared by dissolving Rhodamine 123 (Sigma Aldrich 83702) in an acetone/ethanol mixture solvent (5/1 in volume), followed by uniformly dispersing 1 mL Rhodamine solution in ~5 mL melting paraffin wax. The Rhodamine-marked paraffin wax was used to prepare the composite strip and can be detected by fluorescence microscope and laser scanning confocal microscopy.

**1.5 Characterization.** The structures were characterized by scanning electron microscopy (SEM) (Hitachi FE-SEM S-4800 operated at 1 kV) and transmission electron microscopy (TEM, JEOL JEM-2100F operated at 200 kV). The visible light was generated by a solar simulator with AM1.5 solar light (Lansheng XQ350W, Shanghai, equipped with a 350 W Xe lamp and an AM1.5 filter-typical solar spectrum). The near infrared light illumination was obtained by using an LPF772 filter to filter the the light with wavelengths below 772 nm. The light intensity was calibrated using a reference Si solar cell (Oriel-91150). The coefficient of thermal expansion was measured by Thermo Mechanical Analyzer (Mettler Toledo TMA/SDTS841e). Fluorescence microscope (Olympus BX51) was used to monitor the differential expansion of paraffin wax. Three-dimensional confocal microscopy image was generated by a laser scanning confocal microscope (Nikon C2<sup>+</sup>).

## **2. Simulation of a spontaneous curvature model for the CNT-based photo-responsive strip**

**2.1 Free energy of the composite strip.** According to our experiment, the polyimide substrate is reluctant to deform, so we can assume that it does not stretch or shrink when it is exposed to light. On the contrary, the CNT film may be considered as a two-dimensional anisotropic material and it has been found upon heating, the CNT film might shrink along the CNT-aligned direction while swell across the CNT-aligned direction. The deformation of the composite material is mainly due to the differential expansion between the top and bottom layers of the film. Although the bending rigidity of the material itself might affect bending deformation to some extent, it would not play the central role when the two layers show similar bending rigidity. Therefore, for simplicity, the bending rigidity of the composite material can be neglected in this simulation.

Firstly, we focus on the direction across the CNT-aligned direction. We assume its original width at the initial temperature  $T_0$  is  $L_0$ , upon heating to the temperature  $T$  it might stretch to  $L(T)$  which obviously depends on the  $T$ . However, the film is not freely

stretching but attached to the polyimide, so its final width  $L_r$  might differ from  $L(T)$ , which could cause an energy jump  $\Delta F$  from its minimum energy state. By Hooke's law,

$$\begin{aligned}\Delta F &= \frac{k}{2}(L_r - L(T))^2 = \frac{kL_0^2}{2}\left(\frac{L_r - L_0}{L_0} - \frac{L(T) - L_0}{L_0}\right)^2 \\ &= \frac{M}{2}(\varepsilon - \varepsilon_0)^2\end{aligned}\quad (1)$$

where we define the strains  $\varepsilon = (L_r - L_0)/L_0$  and  $\varepsilon_0 = (L(T) - L_0)/L_0$ .

Therefore, if we also take into the consideration the CNT-aligned direction and shearing strains, the free energy of a deformed CNT film at temperature T can be expressed as

$$F = \frac{M_x}{2}(\varepsilon_{xx} - \varepsilon_{xx0}(T))^2 + \frac{M_y}{2}(\varepsilon_{yy} - \varepsilon_{yy0}(T))^2 + M_{xy}\varepsilon_{xy}^2 \quad (2)$$

where  $\varepsilon_{xx}$  and  $\varepsilon_{yy}$  are the strains along and across the CNT-aligned direction, respectively, while the last term accounts for the shearing contribution.  $M_x$ ,  $M_y$  and  $M_{xy}$  are the three corresponding moduli.

The above situation might be dramatically changed after illumination: CNT/paraffin wax composite layer anisotropically expanded locally while the polyimide substrate is reluctant to deform; the combining effect causes the composite film to bend locally which effectively imposes a local spontaneous curvature to the composite film. See Fig. S14 (left) for example, after heating the paraffin substrate remains at  $L_0$  while the CNT stretches to  $L$ ; in order to prevent the CNT from being detached from the paraffin the composite film has to bend towards the paraffin side to some extent. The geometry relations can be simply read from the Fig. S14:

$$\frac{d + R}{R} = \frac{L}{L_0}$$

therefore

$$\frac{d}{R} = \frac{L - L_0}{L_0} \Rightarrow cd = \varepsilon \quad (3)$$

where  $c \equiv 1/R$  is the curvature of the CNT film. Obviously, Equation (3) sets up the relationship between the bending curvature and the strain of the film, and it can be used to turn the mechanical model of Equation (2) into a geometrical model of Equation (4). Actually, this model is also known as double-layer model or area-difference elastic membrane model in the classic membrane elastic theory<sup>S1</sup>

However, our system is different from that of the bio-membrane. Firstly, according to our experiment the polyimide film highly resist the shearing deformation. Therefore, the deformation of the composite film should preserve the Gaussian curvature of the original shape ( $K = c_1 \times c_2$ , where  $c_1$  and  $c_2$  are the two principal curvatures of the film,

respectively). In our experiment the initial  $K$  is zero, and it indicates only one of the two principal curvatures can survive, which is assumed to be along the  $\gamma$  direction as shown in Fig. S14. Secondly, the local strains within the film might not be the same across the film since the temperature distribution is not perfectly uniform. This will cause the film to have different local spontaneous curvatures across the film. The above discussion indicates that the previous free energy can be re-written as follows

$$F = \int \frac{\kappa_X}{2} [c(\gamma) \cos^2 \theta - c_X(s, \tau)]^2 ds d\tau + \int \frac{\kappa_Y}{2} [c(\gamma) \sin^2 \theta - c_Y(s, \tau)]^2 ds d\tau \quad (4)$$

$$+ \int G c^2(\gamma) \cos^2 \theta \sin^2 \theta ds d\tau$$

Along each direction, the free-energy form is similar to the Helfrich free energy<sup>S2</sup> that has been successfully used to explain the formation of the biconcave shape of the red blood cell. Compare Equations (3), (4) with Equation (2), it is easy to find

$$\kappa_X = M_x d^2$$

$$c(\gamma) \cos^2 \theta d = \varepsilon_{xx}$$

$$c_X d = \varepsilon_{xx0}(T) \quad (5)$$

Similar relations hold for the  $y$  direction and the shearing contribution.

In this model, the film with size of  $a$  by  $b$  is parametrized by parameters  $s$  and  $t$ . The direction of the non-vanishing principal curvature is parametrized by parameter  $\gamma$  which is related to  $s$  and  $t$  by

$$\gamma = s \cos \theta + t \sin \theta. \quad (6)$$

The equilibrium shape of the film can be determined by minimizing the free energy of Equation (2) with respect to  $c(\gamma)$  and  $\theta$ .

It can be proved that the bending direction can only be paralleled or perpendicular with the orientation of CNTs for the case of  $c_X < 0$  and  $c_Y < 0$ , i.e.,  $\theta = 0$  or  $\theta = \frac{\pi}{2}$ .

**2.2 The role of the temperature distribution.** We found that when light is on, the temperature distribution plays an important role in determining the bending direction of the film. Therefore, we assume that the bending moduli and spontaneous curvatures depend on the temperature as follow

$$\kappa_X(T) = \kappa_{X0} + \frac{(\kappa_{X1} - \kappa_{X0})(T - T_0)}{(T_1 - T_0)}, \quad \kappa_Y(T) = \kappa_{Y0} + \frac{(\kappa_{Y1} - \kappa_{Y0})(T - T_0)}{(T_1 - T_0)}$$

$$c_X(T) = c_{X0} + \frac{(c_{X1} - c_{X0})(T - T_0)}{(T_1 - T_0)}, \quad c_Y(T) = c_{Y0} + \frac{(c_{Y1} - c_{Y0})(T - T_0)}{(T_1 - T_0)} \quad (7)$$

According to the experimental results, we may obtain,

$T_0 = 25^\circ, T_1 = 45^\circ, \kappa_{x0} = 2\kappa_{y0}, \kappa_{x1} = 1.5\kappa_{y0}, \kappa_{y1} = 0.2\kappa_{y0}, G = 25\kappa_{y0},$   
 $c_{x0} = 0, c_{x1} = -0.043\text{nm}^{-1}, c_{y0} = 0$  and  $c_{y1} = 0.06\text{nm}^{-1}$ . (The bending modulus  $\kappa_{y0}$   
is of the dimension of energy and has been taken as the unit energy.)

The dynamical evolution of the temperature is governed by the following equation

$$\frac{\partial T(s, \tau)}{\partial t} = a\nabla^2 T + Q_L(s, \tau) - q_D(s, \tau)(T - T_0) \quad (8)$$

where  $a$  is the thermal diffusivity of the composite material,  $Q_L$  is the input heat due to the light and the last term accounts for the heat being diffused into the environment per unit time which is assumed to be proportional to the temperature difference.

Based on Equations (4)-(8), the simulations are performed according to the following procedure. (i) It starts with an initial temperature and a given size of film, and Equation (8) is firstly used to evolve the temperature distribution. (ii) After the temperature distribution is obtained at every time step, the local elastic properties of the composite film or strip are evaluated by Equation (7), which will be further inserted into Equation (4) to minimize the free energy of the system in order to determine the optimized shape of the film. (iii) The above two steps are repeated until the temperature does not evolve anymore. Two typical simulation results are shown in Fig. S15 which can be directly compared with experimental measurements.

Actually, Strips A and B shared the material and configuration except different aspect ratios. Therefore, the aspect ratio was the key factor for the bending competition. It is obvious that the temperature distribution is not uniform especially at the beginning (also see the experimental data in the main text). We hypothesize that this uneven distribution of temperature is responsible for the selective photo-responsive actuation (apheliotropic or phototropic) of the film to the light for different a/b ratios. To confirm this hypothesis, we calculate the free energies of different a/b ratios at  $t = 0.02\text{s}$  for apheliotropic and phototropic bending cases, respectively. The result clearly indicates that, for lower b/a ratios, phototropic bending is more favorable; while for higher b/a ratios, apheliotropic bending becomes a better choice (Fig. S16).

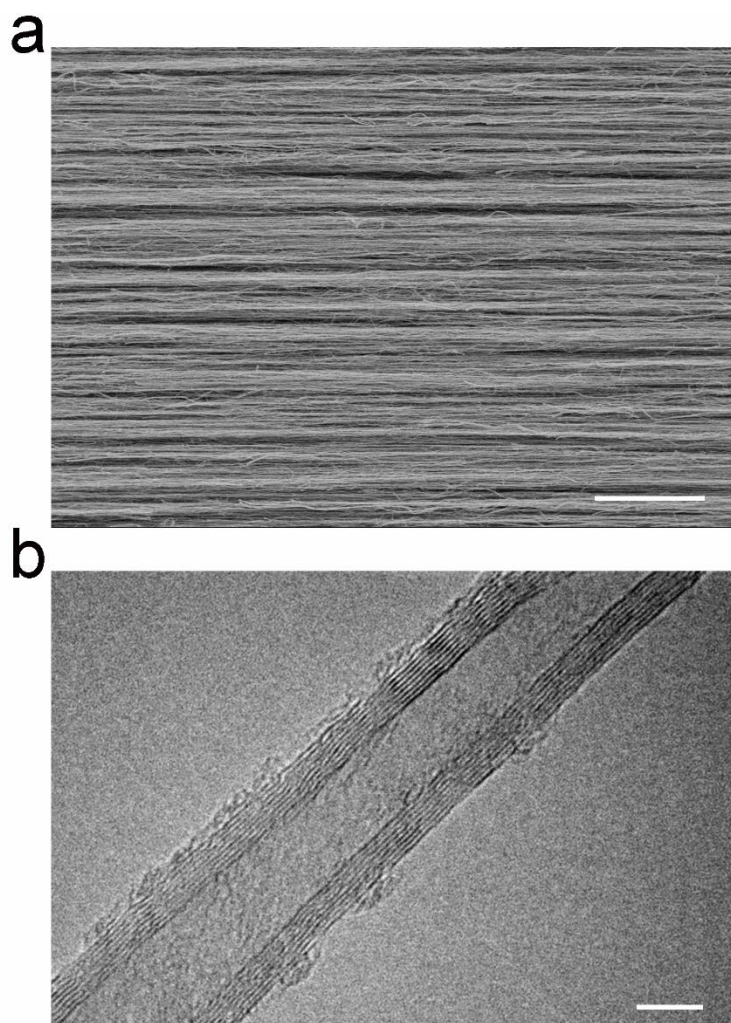


**Figure S1.** (a) SEM image of aligned CNTs. (b) TEM image of a CNT with a multi-walled structure. Scale bar, 50  $\mu\text{m}$  for (a) and 5 nm for (b).

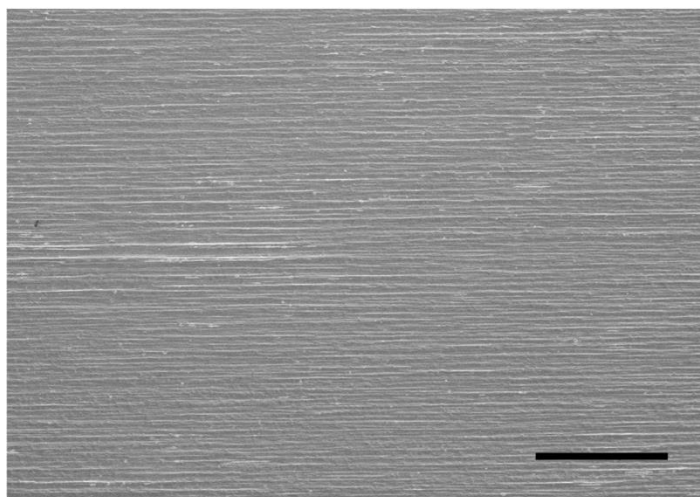


**Figure S2.** SEM image of a paraffin wax/CNT layer by a top view. Scale bar, 200  $\mu\text{m}$ .

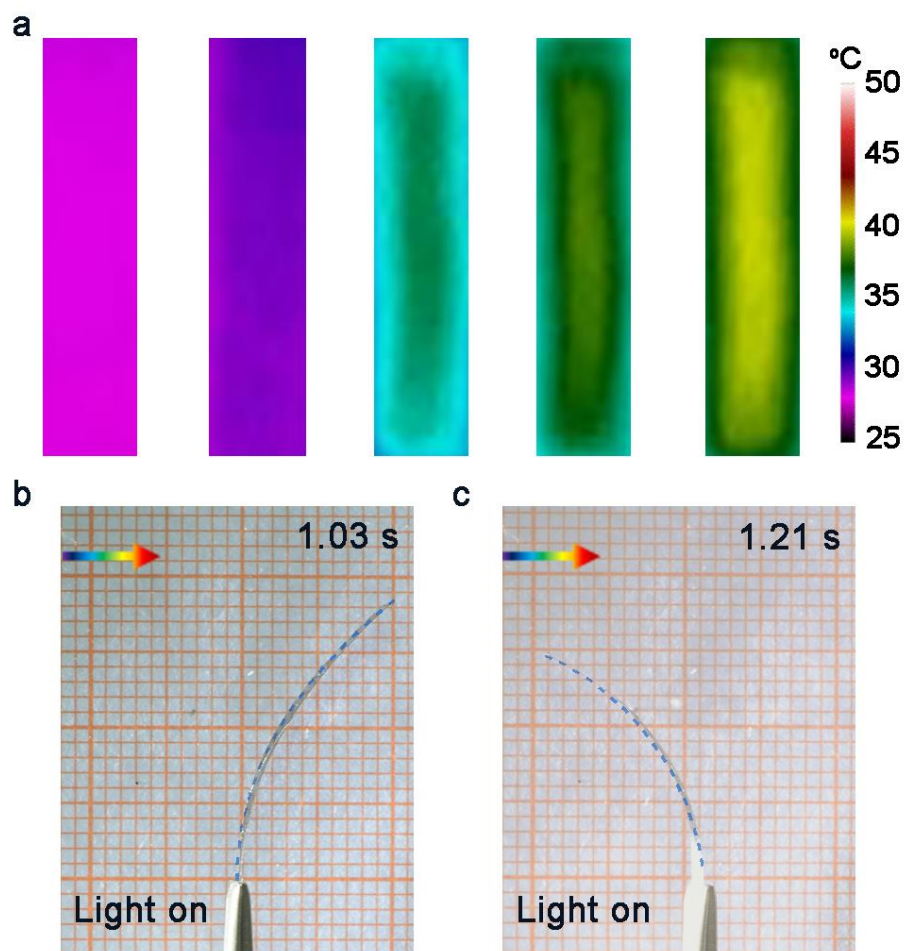


**Figure S3.** (a) Infrared images of a CNT/paraffin wax/polyimide composite strip after near infrared light illumination (wavelength,  $>772$  nm). (b) and (c) Photographs of Strips A and B in response to near infrared light, respectively (the light was illuminated from the left with an intensity of  $50 \text{ mW cm}^{-2}$ ).

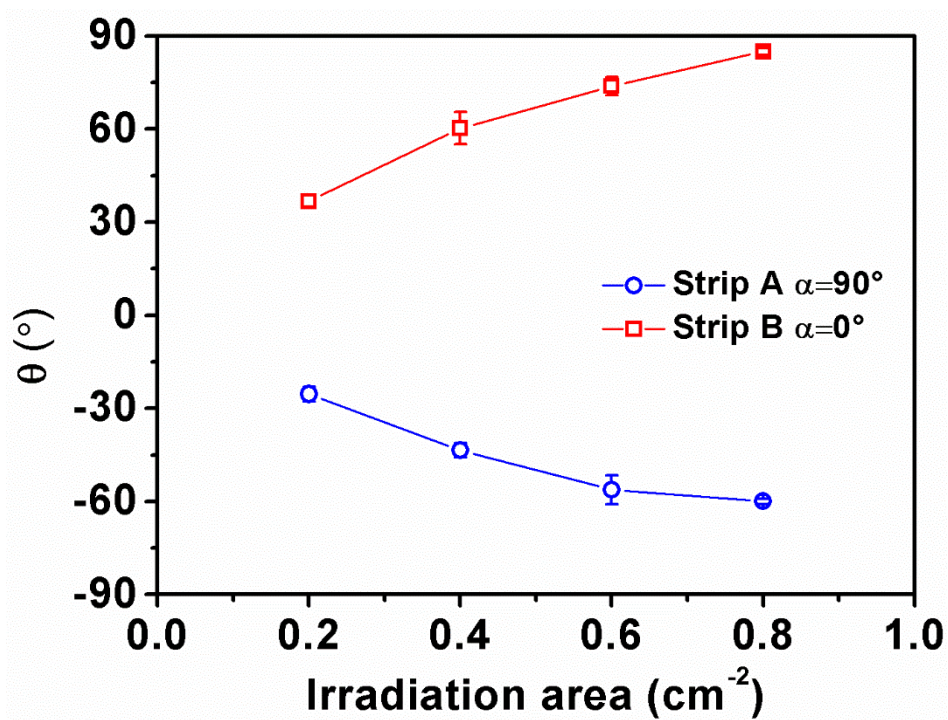


**Figure S4.** Dependence of the bending angle on the irradiation area for Strips A and B.

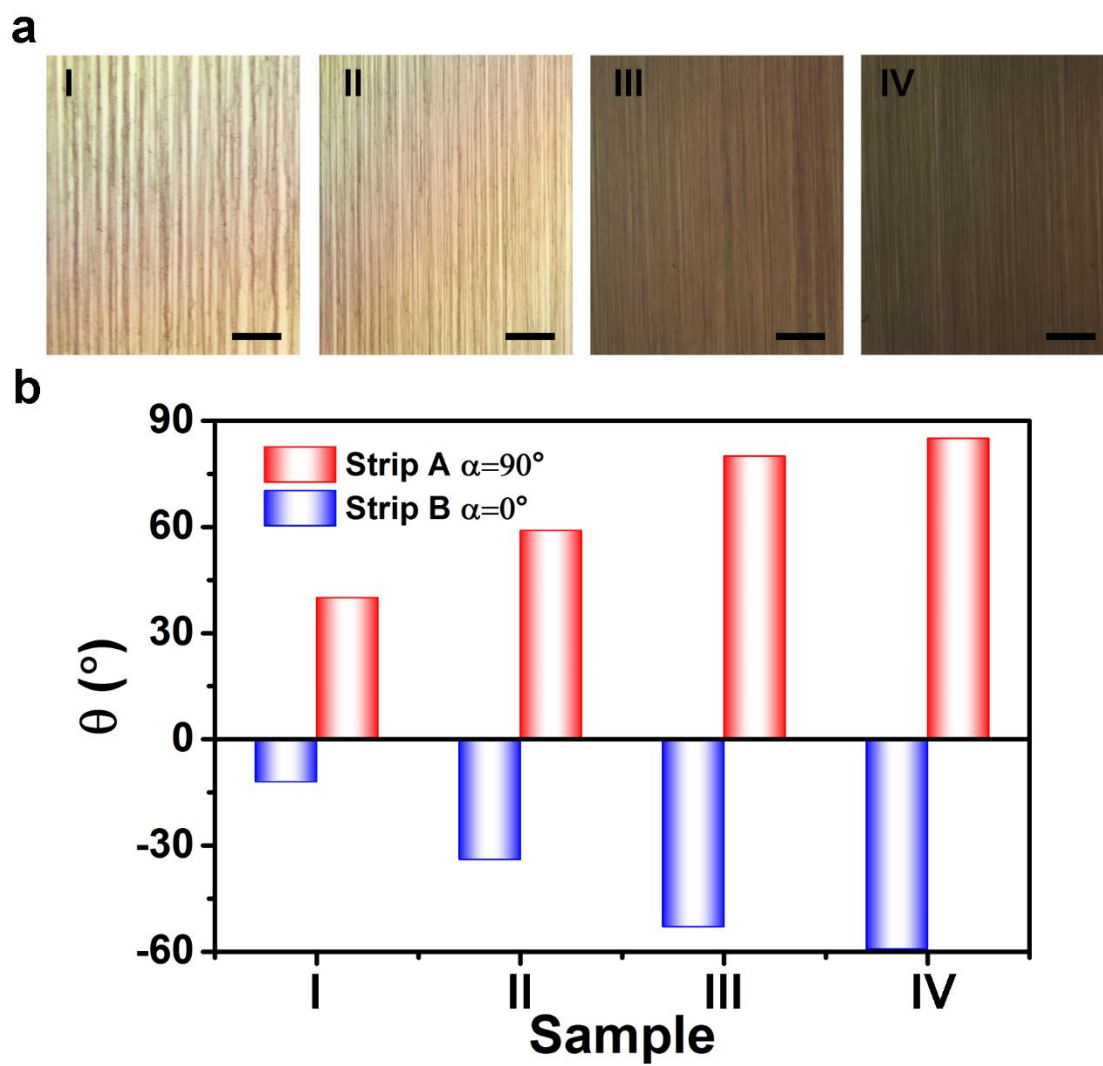


**Figure S5.** (a) Micrographs of aligned CNTs with different sizes of voids. (b) Dependence of the bending angle on the void size for Strips A and B.

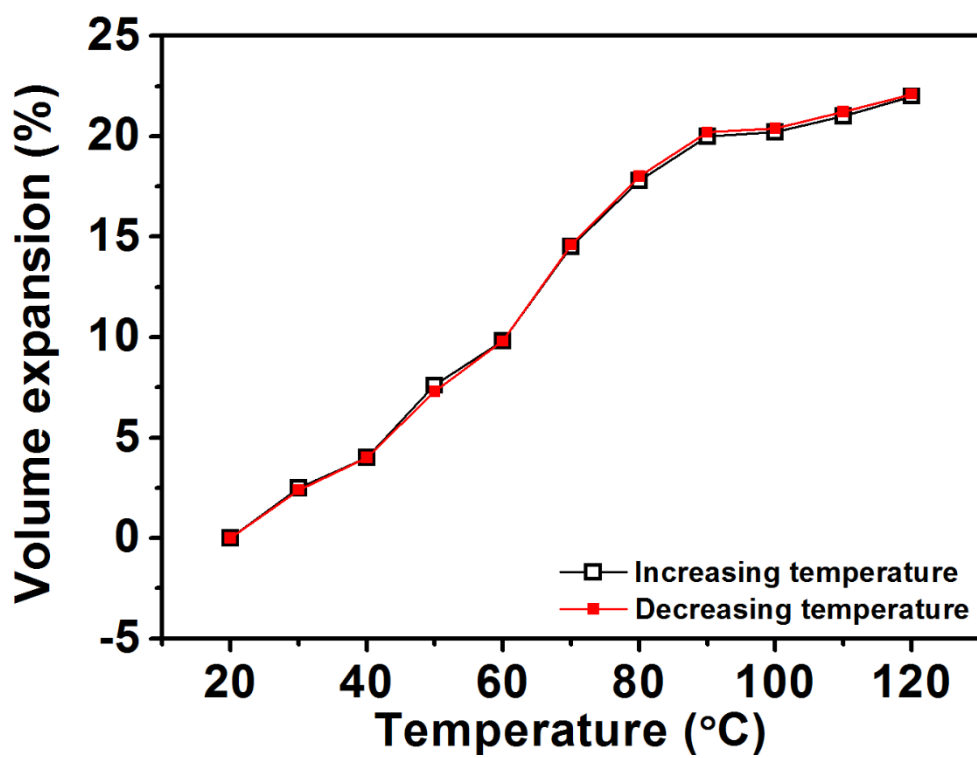


**Figure S6.** Dependence of volume expansion of paraffin wax on temperature.

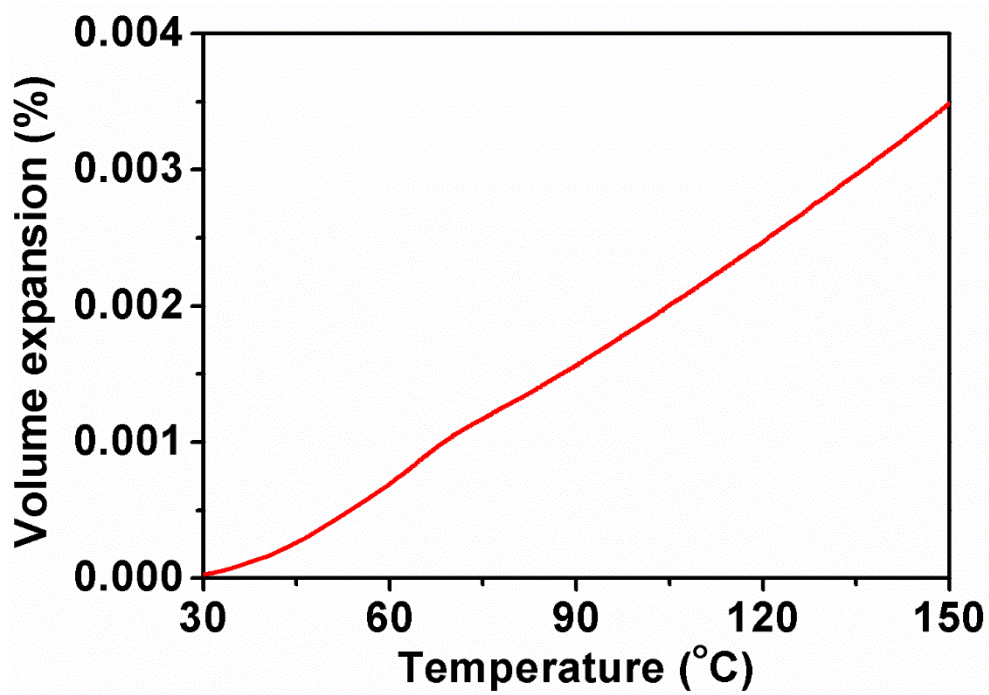


**Figure S7.** Dependence of volume expansion of polyimide on the increasing temperature.

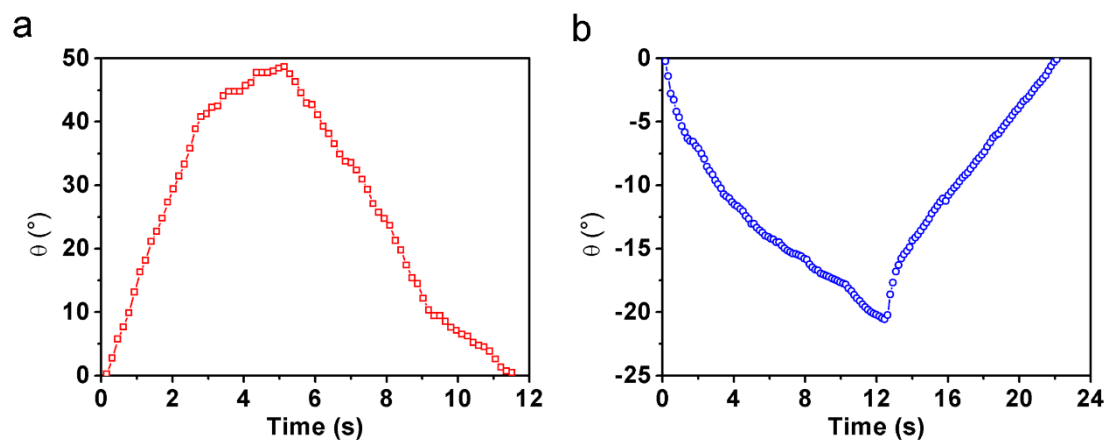


**Figure S8.** Dependence of bending angle on operation time for Strips A (a) and B (b) based on polydimethylsiloxane.

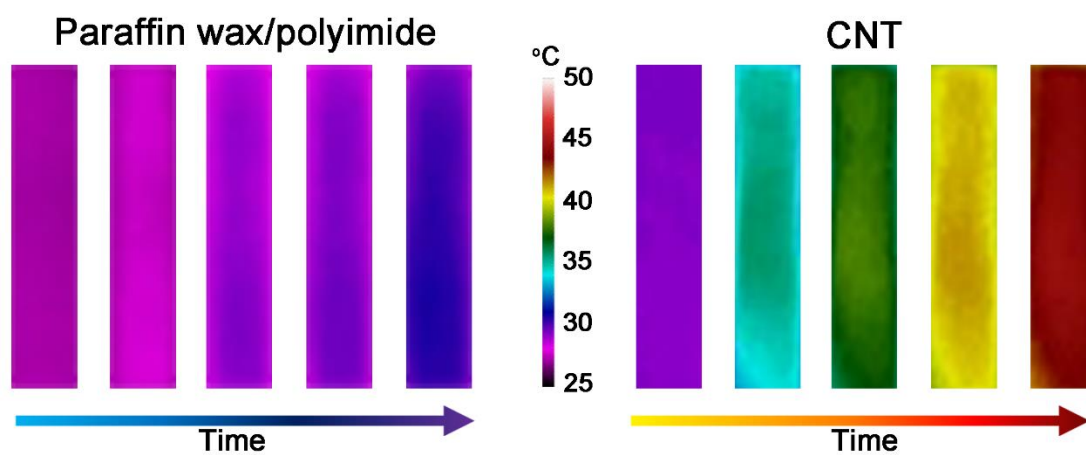


**Figure S9.** Infrared images of a paraffin wax/polyimide composite strip and pristine CNTs after visible-light illumination (light intensity of  $100 \text{ mW cm}^{-2}$ ).

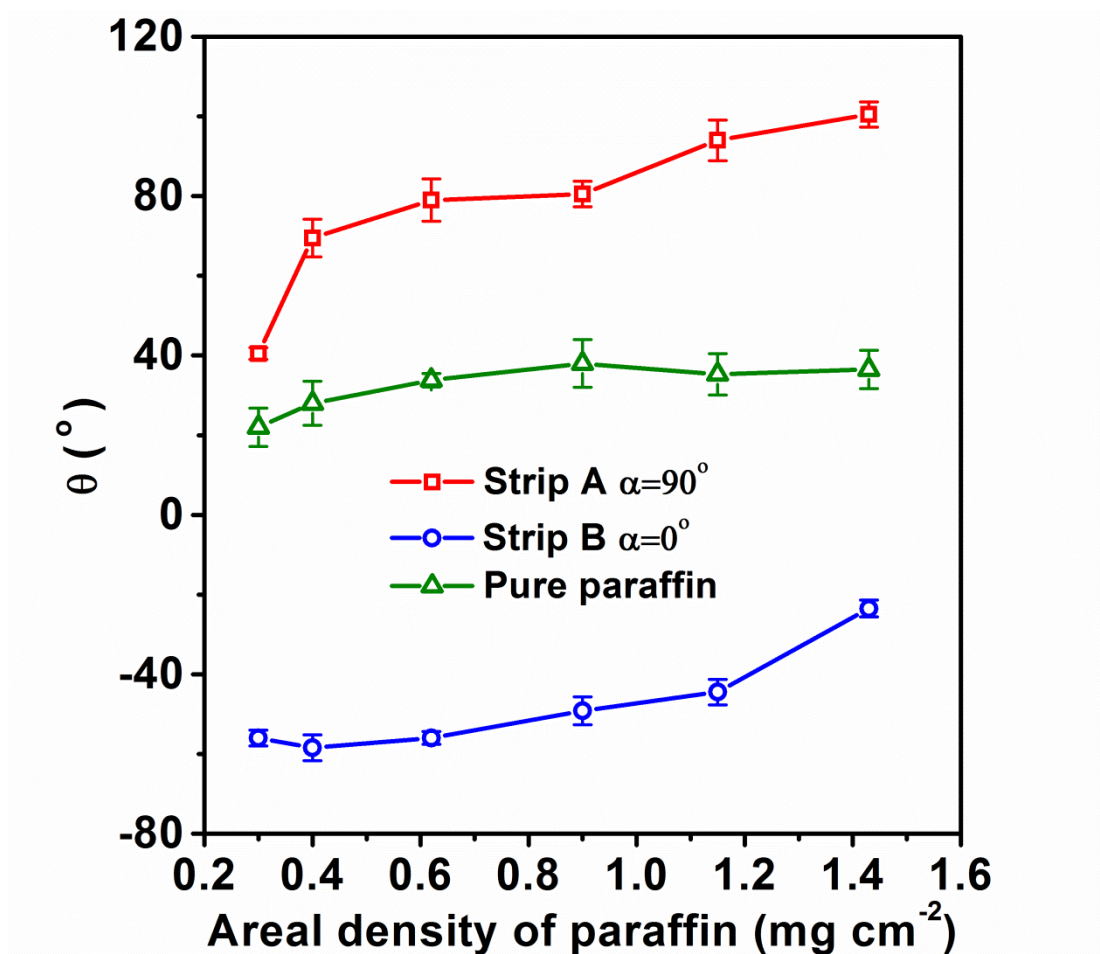


**Figure S10.** Dependence of bending curvature on the areal density of paraffin wax for Strip A, Strip B and strips without aligned CNTs.

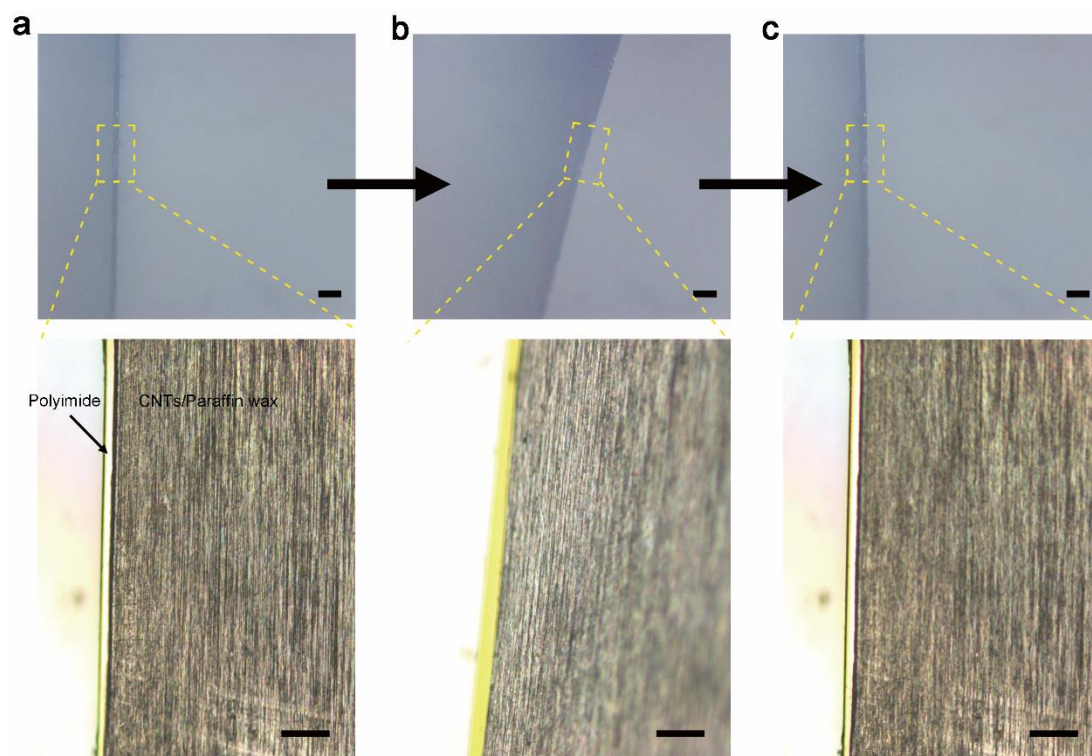


**Figure S11.** Micrographs of an aligned CNT/paraffin wax/polyimide composite layer before (a), during (b) and after (c) deformation at low and high magnifications, respectively. Scale bar, 100  $\mu\text{m}$ .

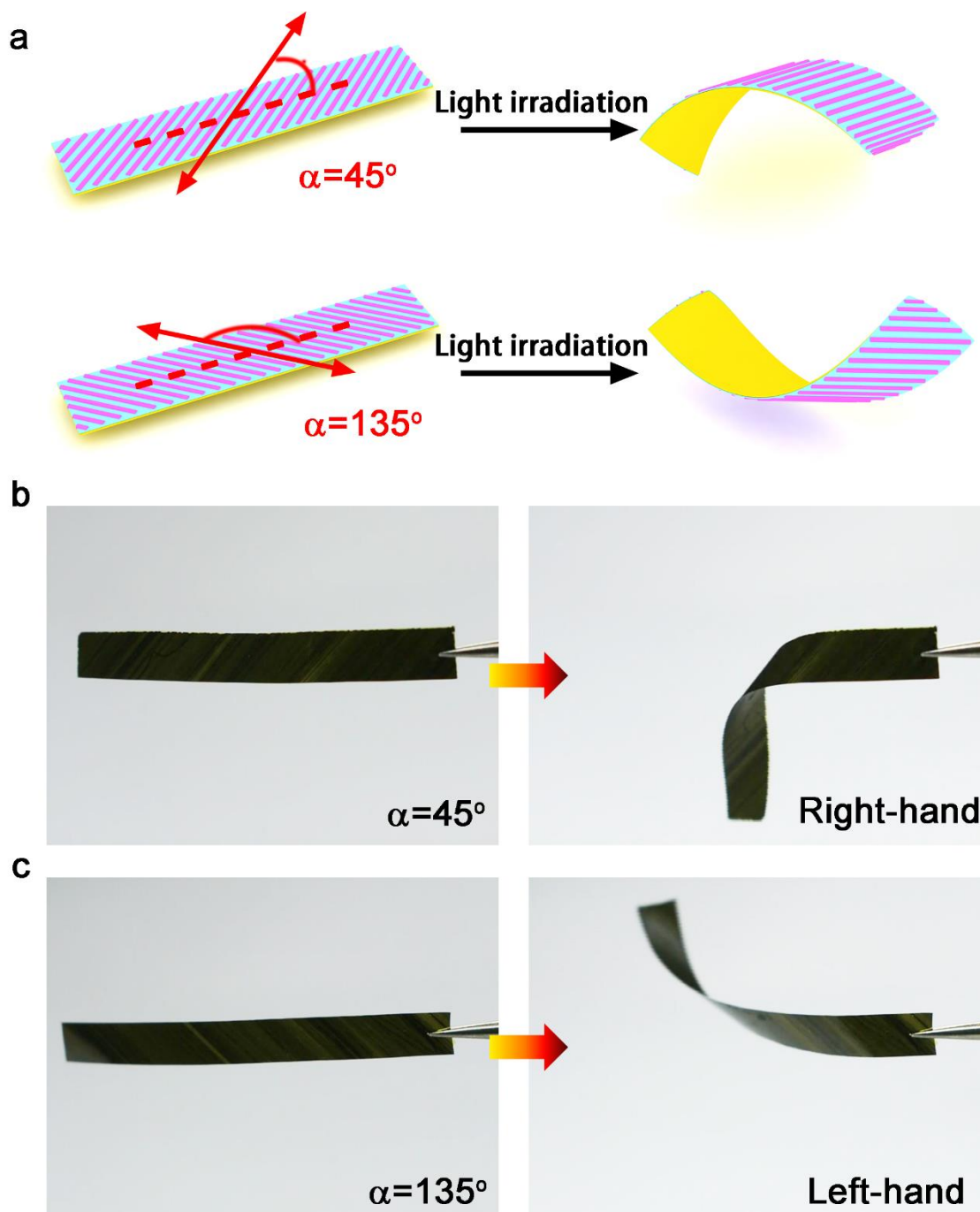


**Figure S12.** (a) Schematic illustration to the right- and left-handed deformation of the composite strips with  $\alpha$  of  $45^\circ$  and  $135^\circ$ . (b and c) Photographs of composite strips with  $\alpha$  of  $45^\circ$  and  $135^\circ$  in response to the visible light, respectively.

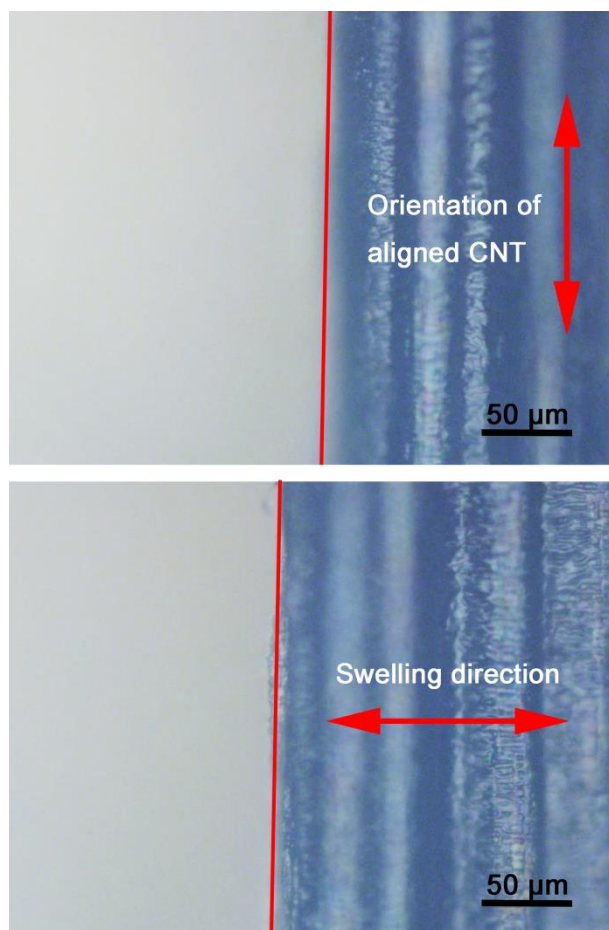


**Figure S13.** Micrographs of an aligned CNT/paraffin wax composite film (1 cm×1 cm) with increasing temperatures from 5 to 35 °C. The edge was expanded by 28 μm.

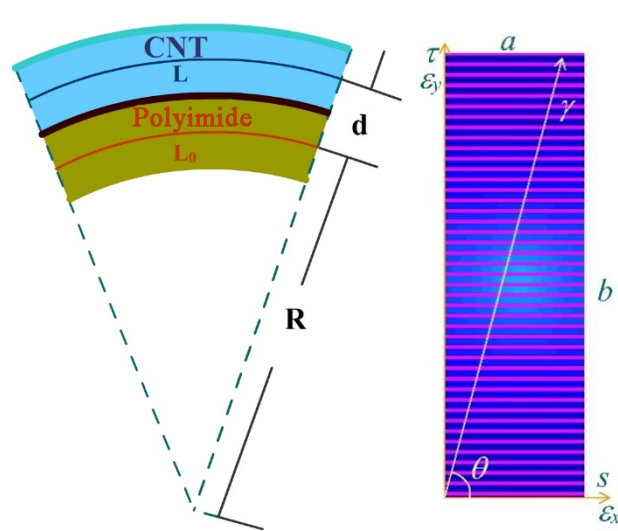


**Figure S14.** Illustration of the model for the simulation.

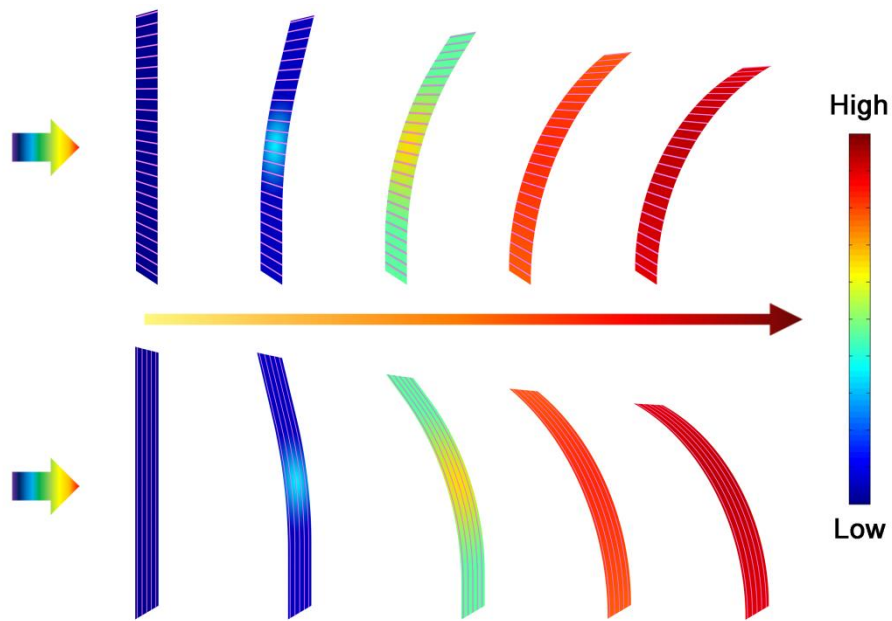


**Figure S15.** A typical simulation of apheliotropic and phototropic bending of the Strip A with  $a$  of 4 mm and  $b$  of 20 mm and Strip B with  $a$  of 20 mm and  $b$  of 4 mm in Figure S14.

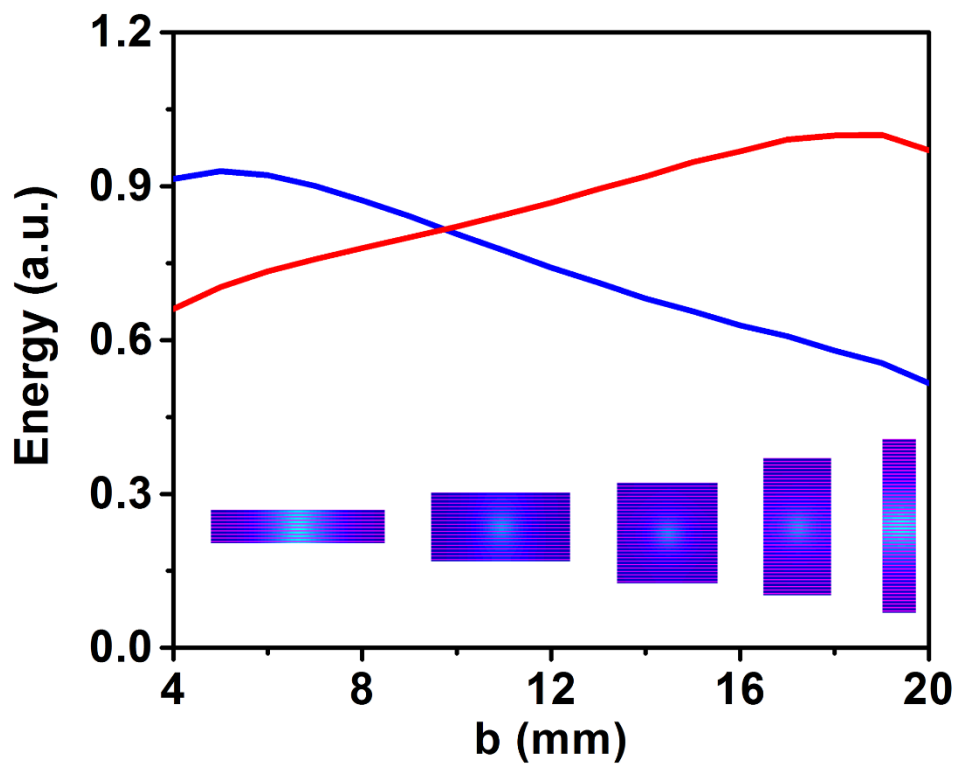


**Figure S16.** Free energy curves of apheliotropic (blue) and phototropic (red) bending as functions of  $b$  with the fixed perimeter of the film ( $a+b=24\text{mm}$ ) according to Figure S14.

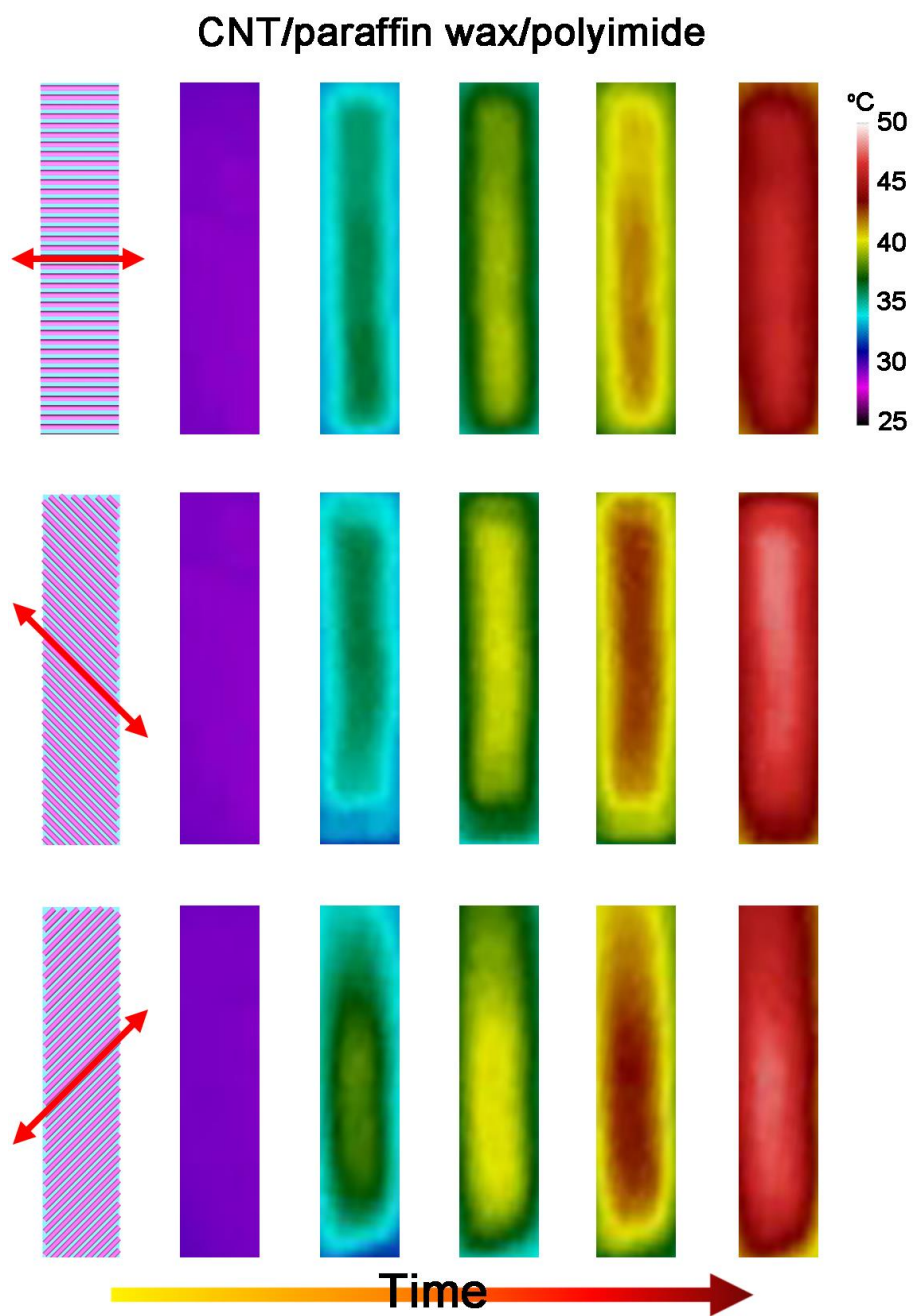


**Figure S17.** Infrared images of CNT/paraffin wax/polyimide composite strips with different aligned directions for the CNTs.

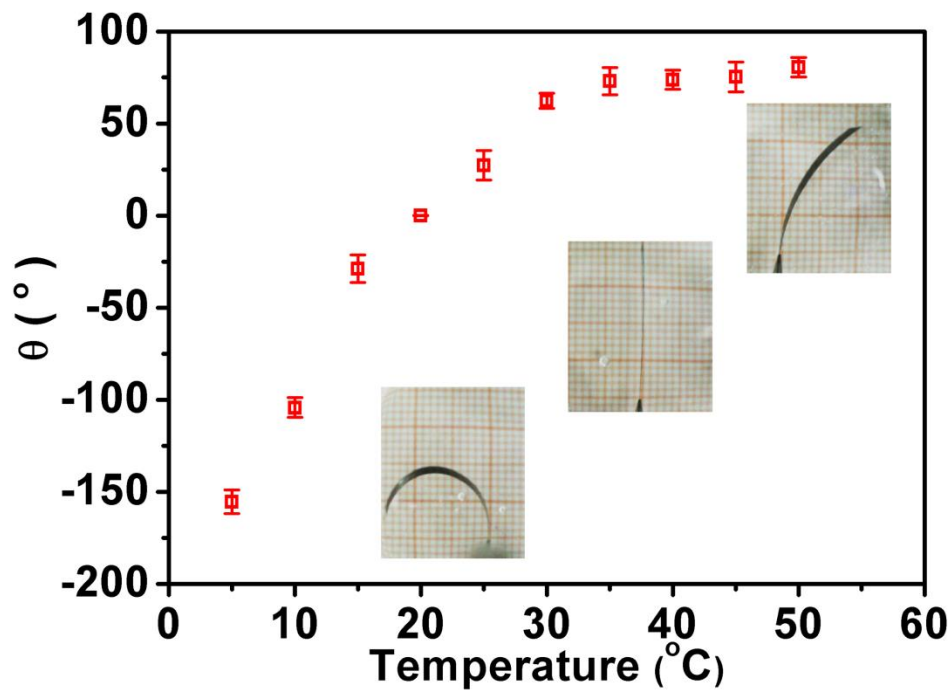


**Figure S18.** Dependence of maximal bending curvature of Strip A ( $\alpha=90^\circ$ ) on temperature. The measurement was performed in the constant temperature environment to investigate the heat effect alone on the actuation.

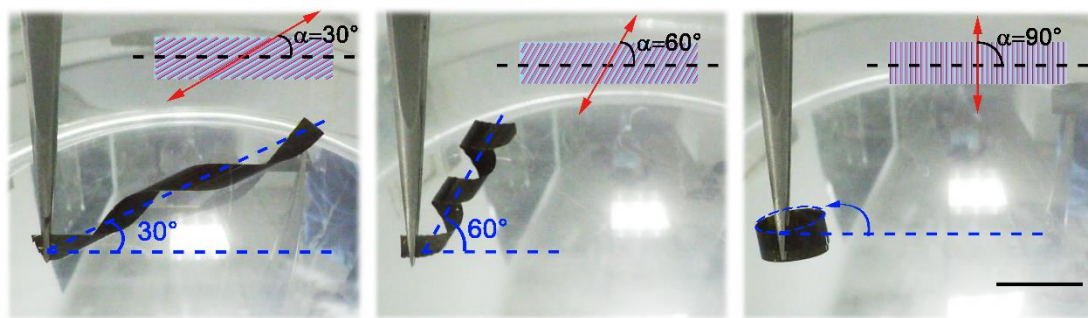


**Figure S19.** Photographs of composite strips with  $\alpha$  of  $30^\circ$ ,  $60^\circ$  and  $90^\circ$  in approaching to the surface of a liquid nitrogen. Scale bar, 10 mm.

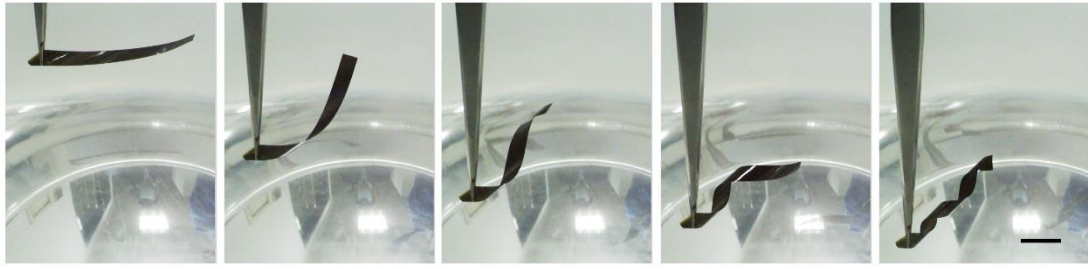


**Figure S20.** Photographs for the shape change of a composite strip with  $\alpha$  of  $45^\circ$  in approaching to the surface of liquid nitrogen.

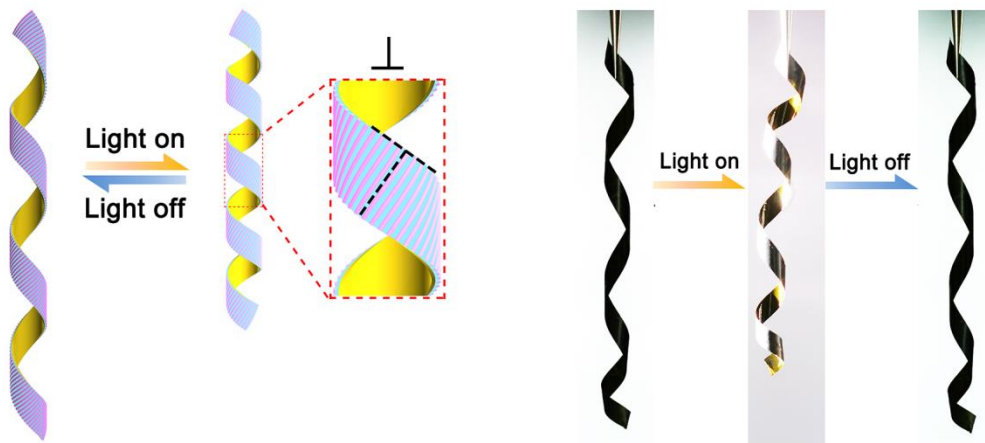


**Figure S21.** Schematic illustration and photographs of a helical actuator thermo-formed by a composite strip with  $\alpha$  of  $90^\circ$ .

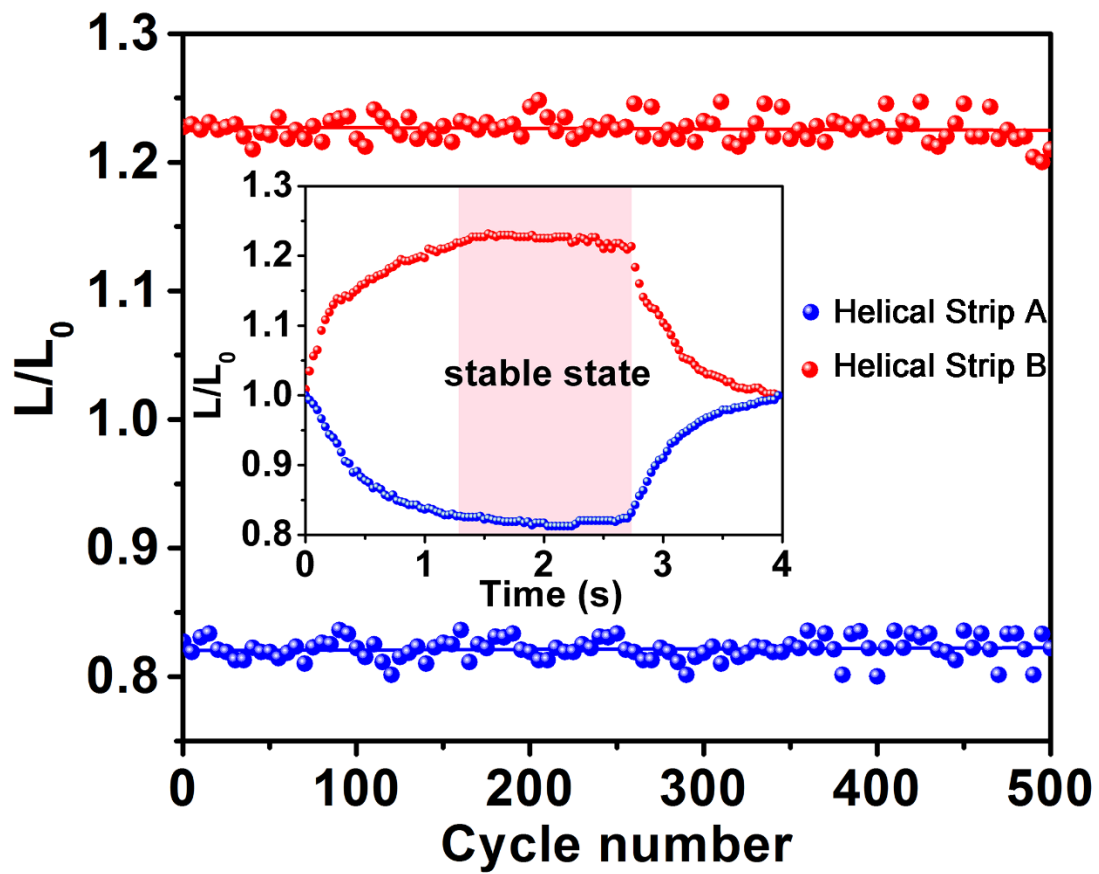


**Figure S22.** Dependence of length change on the illumination cycle number with  $\alpha$  of 0 and 90°. Here  $L_0$  and  $L$  correspond to the length before and after illumination, respectively.

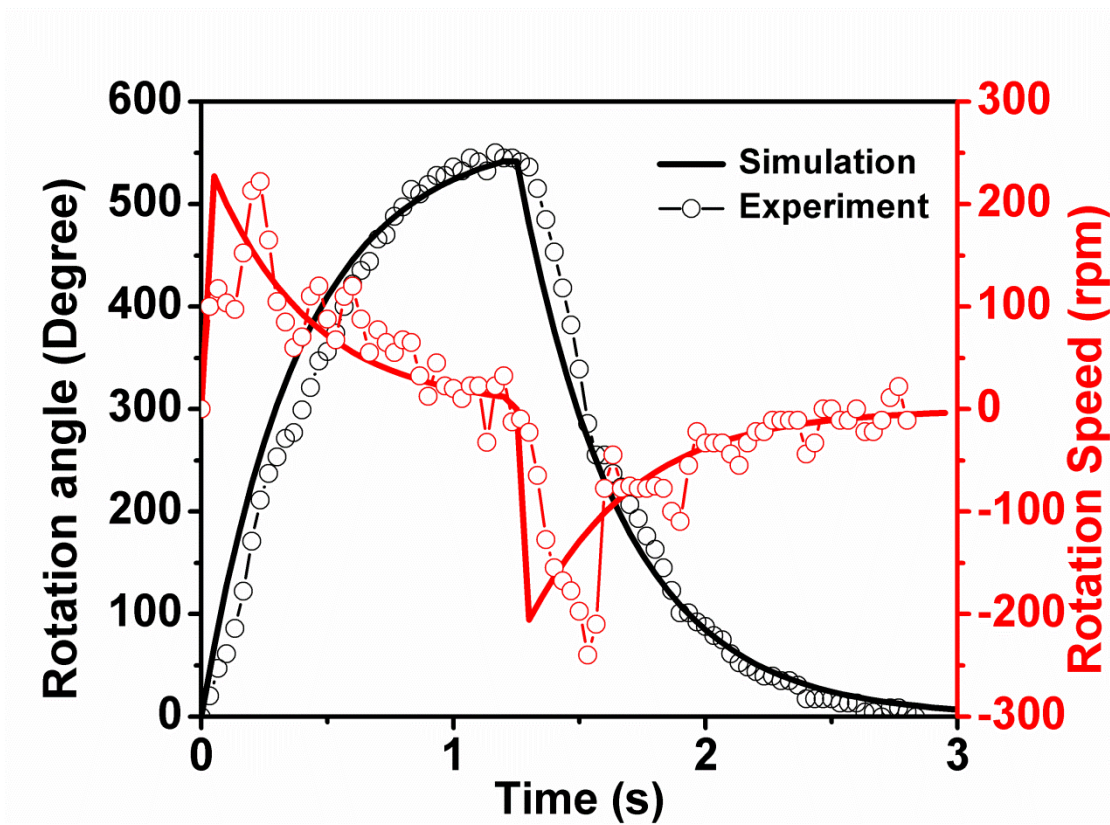


**Figure S23.** Dependence of rotation angle and speed of helical Strip A on the time in a cycle.

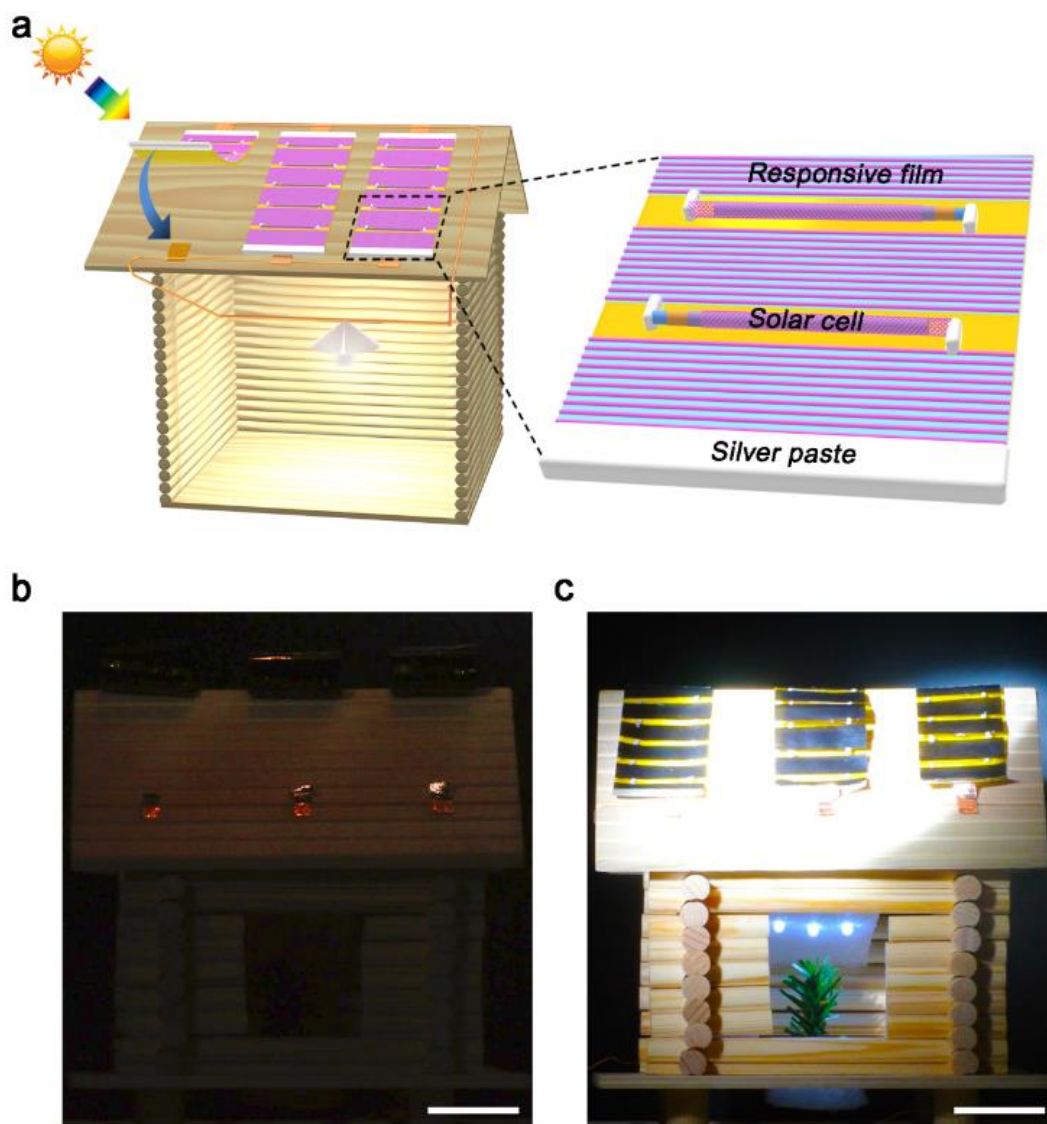


**Figure S24.** (a) Schematic illustration of integration of fibre-shaped perovskite solar cells and a light-responsive actuator. (b) Multi-functional films being curled into cylinders before illumination. (c) Multi-functional films being opened to convert solar energy to electric energy and power the light emitting diode in the room. Scale bars, 3 cm in b and c.

## **Captions for Supplementary Movies**

**Movies S1 and S2.** Apheliotropic and phototropic bending of aligned CNT/paraffin wax/polyimide composite strips.

**Movies S3.** Response of a composite strip with  $\alpha$  of  $45^\circ$  in approaching to the liquid nitrogen.

**Movie S4 and S5.** Twisting and untwisting processes of helical actuators.

**Movie S6.** A light-driving mechanical arm lifting up an object.

**Movie S7.** An Energy harvesting system responding to the visible light and generating electricity.

### Supplementary References

- (S1) Seifert, U. *Adv. Phys.* **1997**, 46, 13.
- (S2) Helfrich, W. *Z Naturforsch C*, **1973**, 28, 693.